Surface & Coatings Technology 294 (2016) 194–200

Contents lists available at ScienceDirect

Surface & Coatings Technology

journal homepage: www.elsevier.com/locate/surfcoat

A high-activity nitrogen plasma flow source for deposition of silicon nitride films

D.Q. Shi, W. Xu, C.Y. Miao, C.Y. Ma, C.S. Ren, W.Q. Lu, Q.Y. Zhang *

[a] Key Laboratory of Materials Modification by Laser, Ion and Electron Beams, Dalian University of Technology, Dalian 116024, China
[b] School of Physics & Opto-electronic Technology, Dalian University of Technology, Dalian 116024, China

ARTICLE INFO

Article history:
Received 20 January 2016
Revised 31 March 2016
Accepted in revised form 1 April 2016
Available online 6 April 2016

Keywords:
Low-pressure plasma flow source
Electrical discharge
Optical emission spectroscopy
Nitrogen dissociation
Silicon nitride

ABSTRACT

We report a tubular plasma source that is capable of creating high-activity nitrogen plasma flow at low pressure. The high-activity nitrogen plasma was produced by a continue low-frequency discharge, in which an intensive pulsed discharge was observed when the electrode was polarized by the positive voltage. Excited at 10 to 115 W, the plasma source allows loading the power density as high as ~80 W/cm^3 to the plasma, producing high-activity nitrogen plasma with a maximum dissociation degree of nitrogen larger than 10%. Based on the tubular plasma source, a special system of plasma enhanced chemical vapor deposition has been developed for deposition of low H-content amorphous hydrogenated silicon nitride (a-SiN$_x$:H) films at room temperature.

1. Introduction

Recently, electric discharges with highly constricted configuration have received much attention because of the potential for a series of novel applications. For example, microdischarges spatially confining the plasma to dimensions of 1 mm or less enable generation of stable glow discharges in a wide variety of gases at atmospheric pressure with as high as 10^{15} cm^{-3} electron density, which is considered applications as plasma cathodes [1]. Atmospheric pressure plasma jet (APPJ) is a facile tool for production of plasma beams and has received much attention due to its prospect in low-temperature processing of materials [2–14]. However, it is generally difficult to deposit high quality of films using an APPJ. It is common knowledge that discharge conditions, such as the working pressure, the discharge configuration, and the excitation way, determine the properties of plasma. At low pressure, the mean free path of molecules and Debye length of electrons are extended to a scale closed to the diameter of APPJ's dielectric tube. Therefore, a low-pressure tube source, which is analogue of APPJ, is particularly interesting to produce high activity of nitrogen plasma for synthesis of nitride films, such as GaN, AlN, and SiN$_x$, which are important in opto-electronic and photovoltaic applications. For example, Czerwiec et al. designed a cylindrical source of inductively coupled plasma (ICP) for generation of plasma beams at low pressure [15,16]. The plasma source is capable of creating high density of nitrogen plasma with an association degree higher than 10%. Henriques et al. studied the nitrogen dissociation of a surface wave driving N_2–Ar discharge in a 0.75 cm quartz tube [17]. Kessels et al. [18–20] developed an expanding thermal plasma source for high-rate deposition of amorphous hydrogenated silicon-nitride (a-SiN$_x$:H) films with plasma enhanced chemical vapor deposition (PECVD) method. In addition, some PECVD systems were developed on the basis of hollow cathode discharge [21].

In this study, we report a low-frequency (20–80 kHz) driving tubular plasma source operating at the pressures ranging from 1 to 200 Pa. This plasma source can be sustained at an intensive discharge state consisting of continue discharge and periodic pulsed discharge when using nitrogen as the working gas, thus creates a high activity of nitrogen plasma. This tubular plasma discharge is rather different from a hollow cathode plasma discharge because we used a dielectric tube confined the plasma and an addition metal rod as the transient cathode. Using the high activity of nitrogen plasma, low H-content amorphous silicon nitride (a-SiN$_x$:H) films were deposited at room temperature in a relatively high rate.

2. Experimental methods

The nitrogen discharge was produced on an experimental setup schematically shown in Fig. 1(a). Fig. 1(b) shows the typical photographs of the bright discharge operating at the given pressures. The plasma source consisted of a quartz tube with inner diameter of 4.0 mm and a 2-mm thick electrode. The electrode was made of stainless steel and driven by a low-frequency AC generator (20–80 kHz) using the vacuum chamber as the ground. The power rating of AC

* Corresponding author at: School of Physics & Opto-electronic Technology, Dalian University of Technology, Dalian 116024, China.
E-mail address: qyzhang@dlut.edu.cn (Q.Y. Zhang).

http://dx.doi.org/10.1016/j.surfcoat.2016.04.002
0257-8972/

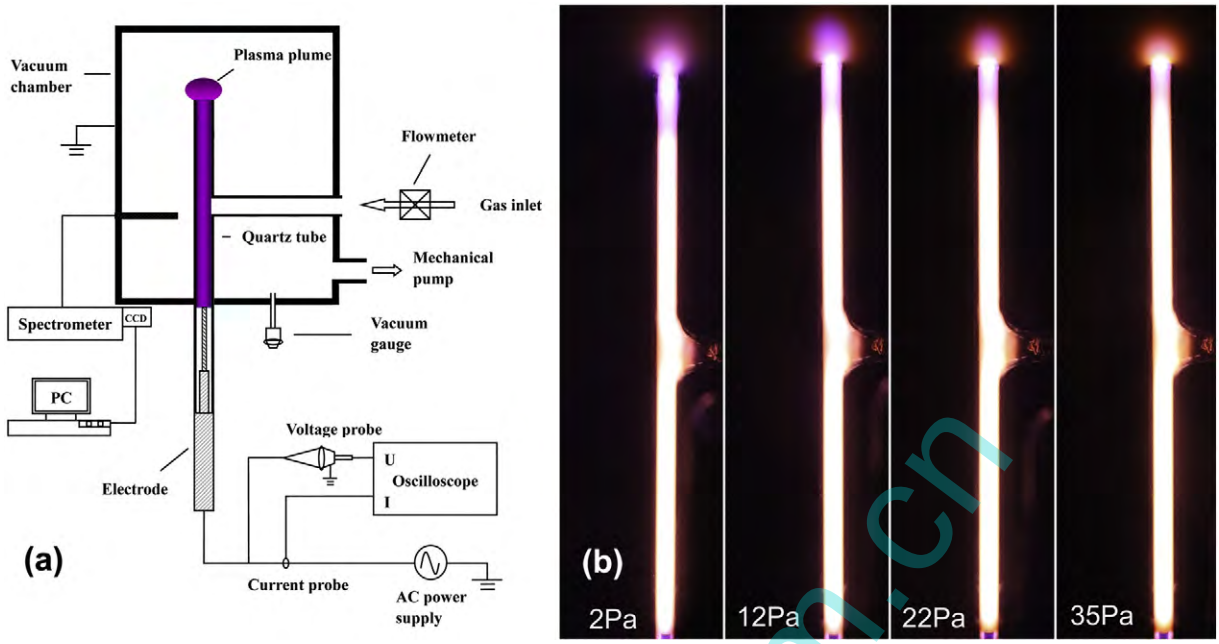

Fig. 1. (a) Schematic experimental setup. (b) Typical photographs of the discharge operating at the given pressures.

generator was 500 W. Before discharging, the chamber was pumped to be better than ~1.0×10^{-3} Pa, and then injected with 12 SCCM 99.999% nitrogen through a gas inlet on the sidewall of the tube. To deposit *a*-SiN_x:H films, a PECVD system was specially designed using a quartz co-axially double tube to replace the single tube for generation of nitrogen plasma. The inner diameters of double quartz tube are 4 and 8 mm, with ~1 mm thick walls, thus pure nitrogen and Ar-diluted 5% SiH_4 are separately fed through the inner and the outer tubes.

Optical emission spectroscopy (OES) was used to study the plasma in the tube. The optical emission was spectrally analyzed in the wavelengths ranging from 200 to 1100 nm using a spectrometer (Acton Research Spectra, Pro-2500i) with a 1200 mm^{-1} grating. The slit entrance was set to ~10 μm, providing a spectral resolution of ~0.05 nm. The electrical characteristics of discharge were measured with a 1:1000 high-voltage probe (Tektronix P6015A 1000×, 3.0 pF, 100 MΩ) and a current probe (Pearson 6600 0.1 V/A) via a digital storage oscilloscope (Tektronix TDS 2012B, 100 MHz, 1 GS/s). In addition, a Langmuir double probe placed at the center of plume, which was ~5 mm away from the nozzle, was used to measure electron density and temperature in the plume.

3. Results and discussion

3.1. Discharge behavior of the tubular plasma

An application of high voltage to the electrode led to breakdown of the gas and creation of plasma confined in the tube. With an increase in input power, the plasma column in the tube gradually expanded along the tube. At a critical voltage, the discharge abruptly produces dazzling-white plasma filling the entire volume, and then a 10–20 mm long plasma plume appears at the tube nozzle, as shown in Fig. 1(b). Fig. 2 shows the typical discharge waveforms of the dazzling-white plasma excited at 115 W. With the sinusoidal excitation, the pattern of the discharge voltage was heavily deformed, and the discharge current exhibited a deformed sinusoidal wave containing the pulsed discharge with extremely high peak current, thus producing a pulse power more than 1 kW within a typical pulse-duty less than 1 μs. The discharge events were highly periodic and the pulsed discharge occurred always at a voltage-rising phase, though the variation in peak current appeared from one cycle of the applied voltage to another. Similar current pulses have been observed in an APPJ excited by AC power supply [4]. In fact, the diffuse plume outside from the tube is very similar to the plume seen when helium APPJ is emerging into helium atmosphere [22]. Differing from the discharge of the APPJ, there is no pulse was observed when the electrode was under the negative polarization. On the other hand, the phase angle between the discharge current and the applied voltage was much smaller than 90° (35°–60°), suggesting the resistive discharge is dominant. The tubular source was very stable and can be sustained for many hours. The plasma source has the advantage in loading sufficient power density to excite

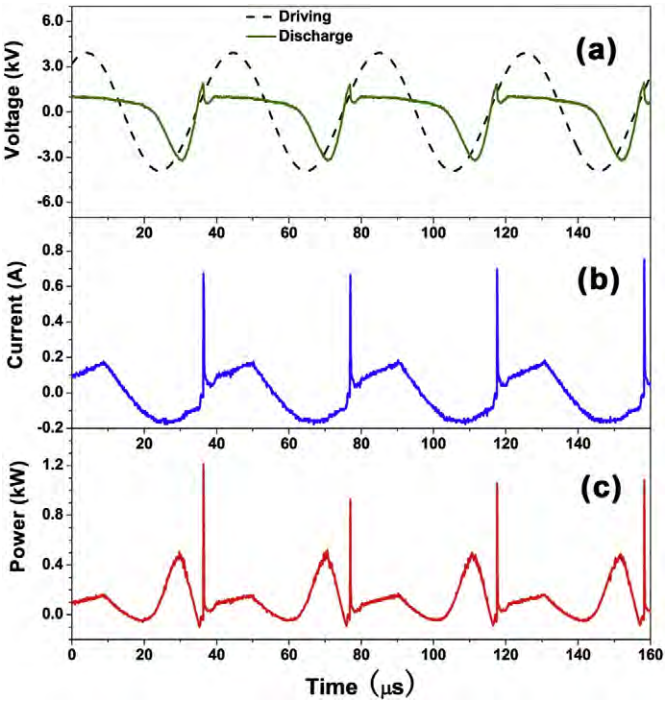

Fig. 2. Typical discharge waveforms, (a) voltage waveforms before and after discharge, (b) current waveform, (c) instantaneous power. The discharge was operated in a 315 mm long quartz tube driven at 12 Pa, 25 kHz, and 115 W.

high-density plasma at low pressure, but no arcing was observed. Using a Langmuir double probe, the density and temperature of electrons in the plasma plume were measured to be 0.9–5.1 × 10^{11} cm^{-3} and 1.62 to 0.55 eV, respectively, with the increase in the input power from ~10 to 115 W [23].

The pulsed discharge events were observed strongly dependent on the discharge conditions, such as the driving frequency, the input power, the effective length of discharge, and the working pressure. For example, using a quartz tube with a 280 mm effective length of discharge, the density of peak current varied in the range of 7–27 A/cm^2 with increasing the input power from 10 to 110 W. When the effective length of discharge was shortened to ~80 mm, an as large as ~430 A/cm^2 peak current was observed at ~90 W, indicating the discharge currents of the periodic pulses are reaching the values corresponding to arcing or transient sparks, thus a high density of plasma is expected on duty of the pulsed discharge. Fig. 3 shows the instantaneous power of the periodic pulses plotted as a function of input power driven at different frequencies. We can see that the pulse power depends on the input power and the driving frequency. Driven at the low frequencies, the pulse power is increasing with the increase in input power. With the increase in driving frequency, however, the increment of the pulse power by increasing the input power changes to be smaller and smaller. At the same time, the maximum input power that could be loaded to the plasma is considerably decreased, probably due to the limit capability of the power supply. At the driving frequencies higher than 40 kHz, a large input power even leads to decrease in pulse power. The critical voltage inducing the pulsed discharge was found decreasing with the increase in driving frequency, as shown in the inset of the figure. Considering that the discharge consists of two regions, namely, the inside and the outside of the tube, we suggest that the pulsed discharge might be related to breakdown of the gas outside the tube [23].

In order to have a comprehensive picture for the low-pressure discharge, the spatial and temporal development of the discharge was studied by registering the optical emission by a photomultiplier tube (PMT). The optical emission was collected by a fiber at different positions along the tube axis and the photocurrent was recorded by an oscilloscope. The photocurrent waveforms at different positions are presented in Fig. 4. For comparison, the discharge current and its integration are also presented in the figure. The time-dependent emission is modulated at the driving frequency (ω) from the region close to the electrode to the plume (Fig. 4a–c), indicating that the light from the discharge plasma is excited once per AC cycle, thus much different from the RF discharge with two parallel electrodes, in which the optical emission was modulated to be 2ω at the center and ω at the electrodes [24]. The modulated emission was ascribed to the excitation at the

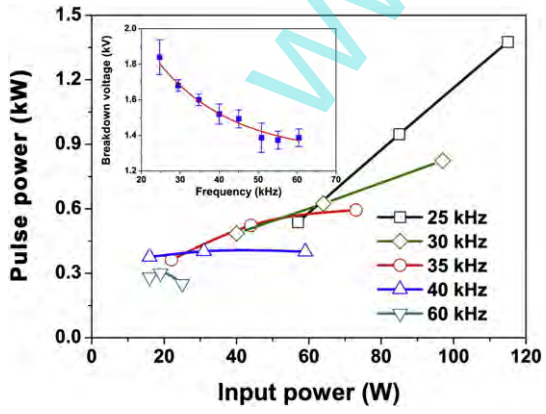

Fig. 3. Instantaneous power of the periodic pulses plotted as a function of input power driven at the given frequencies. The inset shows the breakdown voltage inducing the self-pulsing discharge plotted as a function of driving frequency. The discharge was operated in a 315 mm long quartz tube at 12 Pa.

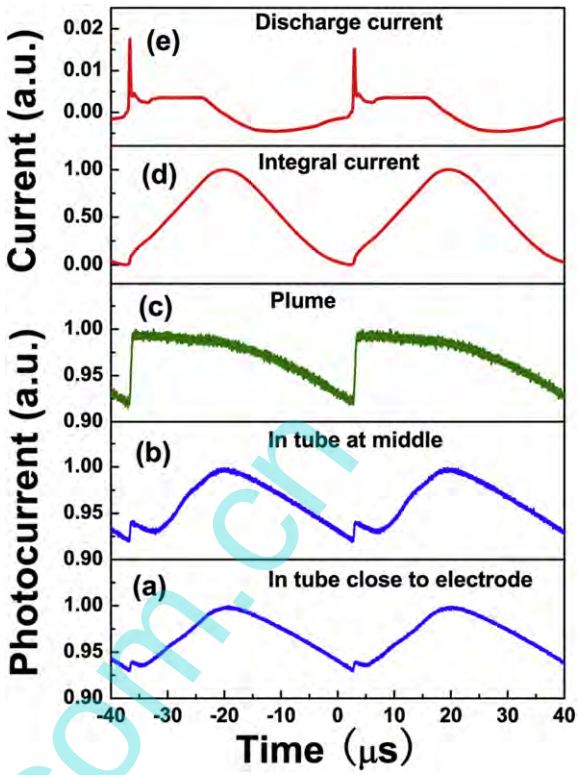

Fig. 4. Photocurrent waveforms collected at the indicated positions in comparison with the discharge current and the integral current waveforms. (a–c) Photocurrents collected at the region close to the electrode, middle, and plume, respectively. (d) Pattern of integral discharge current. (e) Pattern of discharge current. The discharge was operated in an ~110 mm effective length in the tube at ~12 Pa.

electrode regions when the electrodes are polarized by a negative voltage, and then the fast electrons are ejected from the instantaneous cathodes [24]. By integrating the discharge current (Fig. 4e), we found that the pattern of the integral discharge current (Fig. 4d) is highly in accordance with the photocurrents in the tube, except that the photocurrent background is more than 90%. Therefore, we believe that Kuzovnikov and Savinov's mechanism is responsible for the optical emission in the tubular source and the vacuum chamber acts as the instantaneous cathode, because the optical emission was enhanced when it was negatively polarized. Similarly, the pulsed discharge may originate from the ionization enhancement in the gas outside the tube, because the photocurrent enhancement by the pulsed discharge occurs always at a voltage-rising phase and is stronger in the plume than in the tube, thus can be used as the evidence that the ionization wave is initially created by the pulsed discharge in the plume and moves towards the electrode.

3.2. Characterization of the plasma activity

The tubular plasma source is expected to be capable of producing high activity of nitrogen plasma because extremely high power density can be achieved. For example, the power density of plasma excited at 110 W in 280 mm effective length is ~31 W/cm^3, which is about two orders of magnitude higher than that in low-pressure glow discharge. When the effective length of discharge is reduced to 110 mm, the power density of plasma is increased to as high as ~80 W/cm^3. Fig. 5 shows a typical OES of nitrogen plasma in the tube, which was excited at ~98 W within 110 mm effective length of discharge. The optical emissions are assigned to the second positive system (2PS, $C^3\Pi_u \rightarrow B^3\Pi_g$) and the first positive system (1PS, $B^3\Pi_g \rightarrow A^3\Sigma_u^+$) of N_2 molecule, and the first negative system (1NS, $B^2\Sigma_u^+ \rightarrow X^2\Sigma_g^+$) of N_2^+ ions [25]. It is obviously different from the low-pressure glow discharge that the atomic lines from the transitions of N 3p → 3s ($^4S^o$, $^4P^o$, $^4D^o$ → ^4P and $^2D^o$ → ^2P)

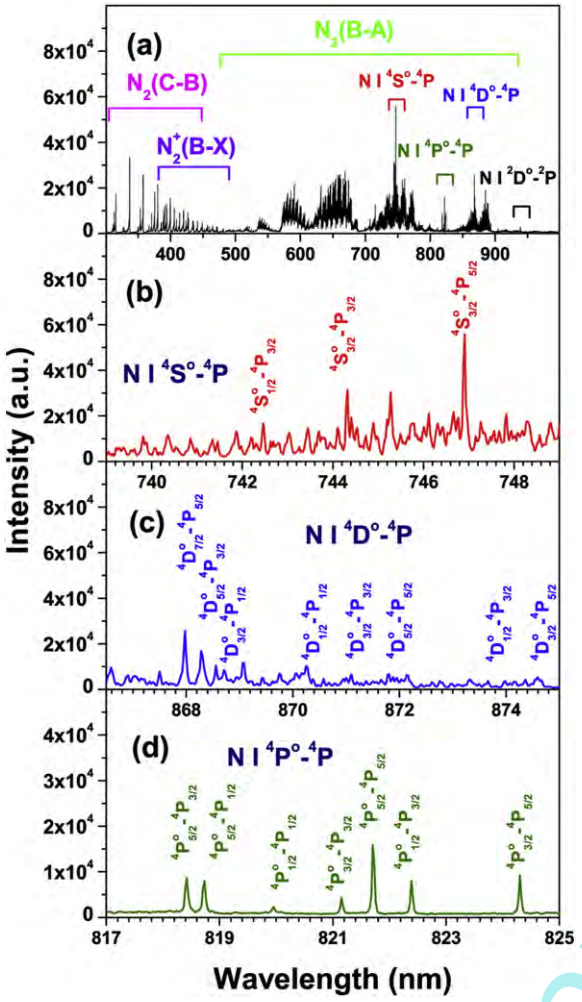

Fig. 5. Typical OES of nitrogen plasma in the tube, which was excited by an input power of ~98 W within 110 mm effective length of discharge.

[26] are extremely intensive, indicating the high dissociation degree of nitrogen molecules.

Using the emission intensities from 2PS and relevant atomic lines, the ratio of atom to molecule densities of nitrogen in the plasma, [N]/[N_2], were estimated by [15–17]

$$R = \frac{[N]}{[N_2]} = \frac{K_{N_2}}{K_N}\frac{A_{N_2}\tau_{N_2}}{A_N\tau_N}\frac{k^X_{N_2}}{k^{dir}_N}\frac{I_N}{I_{N_2}}, \quad (1)$$

where I, A, and τ are the intensity, probability, and radiative lifetime of the optical emission at the specific wavelength, respectively. k is the excitation rate coefficient of the excited state. K is the parameter related to the collection solid angle, the sample volume of the optical emission, and the spectral response. By comparing the intensity of atomic lines from different transitions with Frost et al.'s [27] excitation rate coefficients calculated by R-matrix method, we determined the electron excitation temperatures, and then the excitation rate coefficients of N atom. The excitation rate coefficients of $N_2(C, \nu = 0)$ molecules by electron impact from the ground state $N_2(X)$ were calculated using the excitation cross sections of $N_2(C, \nu = 0)$ recommended by Itikawa [28] under assumption of Maxwellian electron energy distribution function (EEDF). Using these excitation rate coefficients and the parameters listed in Table 1, the [N]/[N_2] values in the plasma were calculated. Fig. 6 shows two examples for determination of the nitrogen dissociation degree in the plasma along the tube axis. In this study, the dissociation degree D_{OES} is defined by

$$D_{OES} = \frac{[N]/2}{[N]/2 + [N_2]} = \frac{R}{2+R}. \quad (2)$$

The dissociation degree determined by the three atomic lines of nitrogen, namely, $^4S^\circ_{3/2} \rightarrow {}^4P_{5/2}$ (746.83 nm), $^4P^\circ_{5/2} \rightarrow {}^4P_{5/2}$ (821.63 nm), and $^4D^\circ_{7/2} \rightarrow {}^4P_{5/2}$ (868.03 nm) is in good agreement with each other. Excited at the approximately equal input powers (68 and 65 W), the averages of dissociation degree over different positions on the axis are 10.6 ± 2.4% and 9.1 ± 1.3% for the discharges operating at 12 and 100 Pa, respectively, indicating that the dissociation degree is predominated by the input power, being consistent with Guerra's simulation for a DC discharge in a tube source [29]. Fig. 7 shows D_{OES} plotted as a function of input power for the discharge driven at different driving frequencies. The dissociation degree is a nearly linear function of input power for the discharges driven at different frequencies.

Besides the high activity, the rotational and vibrational temperatures (T_{rot} and T_{vib}) of the plasma excited in the tube differ from the low-pressure glow discharge. Fig. 8 shows the dependence of T_{rot} and T_{vib} on the input power of the plasma driven at different frequencies. The rotational and vibrational temperatures were obtained by fitting the rovibrational bands in 2PS using the software based on the least-squares fit to an arbitrary function [30]. T_{rot} and T_{vib} of the plasma are input-power dependent, but hardly relating to the driving frequency. The vibrational temperatures are ~5000 K, which is 2000–3000 K higher than those in low-pressure glow discharge. At the given input powers, T_{rot} is monotonically increasing from ~350 to ~680 K, which is in good agreement with our measurement of temperature on the tube wall by a thermal couple. The high rotational and vibrational temperatures are attributed to the high power density dissipated on the plasma. Owing to the small diameter of the discharge tube, it is difficult to determine the electron density of plasma in the tube. For estimation, the electron density (n_e) during the pulsed discharge was calculated by $i = ev_e n_e$ using the current density (i) and assuming the velocity $v_e \sim 10^6$ m/s. The electron density varies in the range of 10^{11}–10^{13} cm^{-3} for the discharge excited at ~10 to 115 W, depending on the power density dissipated on the plasma. This estimation is consistent with the measurement in the plume, thus strongly support that the tube plasma source is capable of creating high density of nitrogen plasma at low pressure.

3.3. Room-temperature deposition of low H-content a-SiN_x:H films

a-SiN_x:H films are important for device passivation, diffusion and oxidation barriers [31]. The deposition of a-SiN_x:H films by conventional

Table 1
Data related to nitrogen atom and molecule in this study.

Species	λ (nm)	Configuration		E_{up} (eV)	τ_{up} (ns)	$A\tau$	K
		Upper	Lower				
N	746.83	3p $^4S^o_{3/2}$	3s $^4P_{5/2}$	11.99 [26]	26.9 [26]	0.528 [26]	0.40
N	821.63	3p $^4P^o_{5/2}$	3s $^4P_{5/2}$	11.84 [26]	10.8 [26]	0.244 [26]	0.30
N	868.03	3p $^4D^o_{7/2}$	3s $^4P_{5/2}$	11.75 [26]	9.86 [26]	0.250 [26]	0.23
N_2	337.1	$C^3\Pi_u, v=0$	$B^3\Pi_g, v=0$	11.16 [25]	36.6 [25]	0.523 [25]	0.16

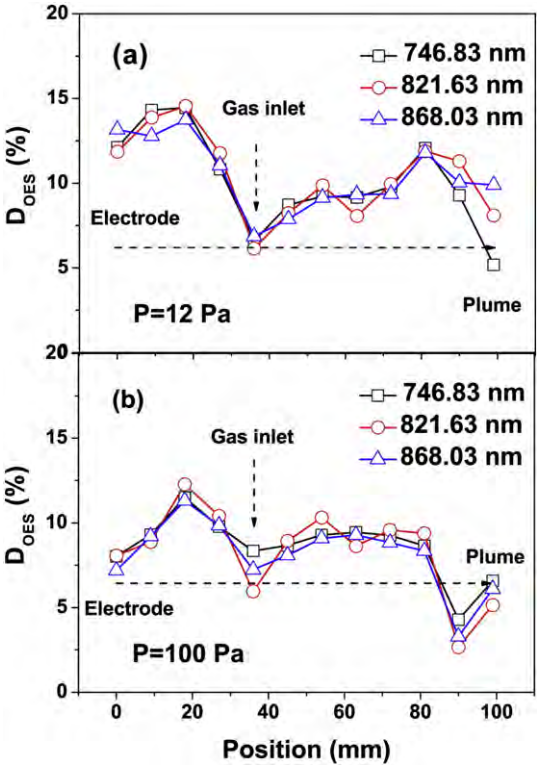

Fig. 6. Examples for determination of the nitrogen dissociation degree in the plasma along the tube axis, (a) 68 W, 12 Pa, and 25 kHz, (b) 65 W, 100 Pa, 25 kHz.

PECVD technology is usually conducted at temperatures higher than 300 °C, thus cannot be used to fabricate organic optoelectronic devices. Therefore, room-temperature deposition of a-SiN_x:H films received much attention in the past decade and PECVD systems based on various plasma sources have been proposed [32–38]. Because these PECVD systems employ SiH_4 and NH_3 as the working gas, the hydrogen content in the a-SiN_x:H films is relatively high [32–38]. On the other hand, a common shortage of these PECVD systems is the low deposition rate at room temperature, generally lower than 30 nm/min. To deposit low H-content a-SiN_x:H films at room temperature, we designed a special PECVD system based on the high activity of nitrogen plasma created by the tubular plasma source. The PECVD system uses a quartz coaxially double tube to replace the single tube for generation of nitrogen

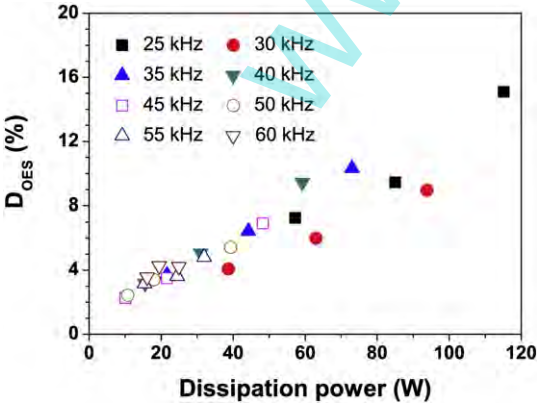

Fig. 7. Dissociation degree of nitrogen plotted as a function of the input power for the discharge excited at the given driving frequencies. The OES was collected at ~30 mm distance to the electrode. The discharge was operated in a 315 mm long quartz tube at 12 Pa.

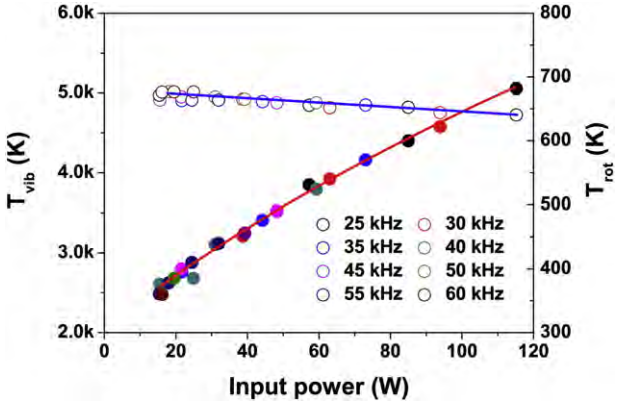

Fig. 8. Dependence of T_{rot} and T_{vib} on the input power of nitrogen plasma driven at different frequencies in a 315 mm long quartz tube at 12 Pa. The OES was collected at ~30 mm distance to the electrode.

plasma by separately feeding pure nitrogen and Ar-diluted 5% SiH_4. The nitrogen in the inner tube is highly associated as well. In addition, the Ar-diluted 5% SiH_4 in the outside tube is partially ionized, thus the a-SiN_x:H clusters are expected to form in the plume, as schematically shown in Fig. 9.

The a-SiN_x:H films were deposited on Si (100) substrate under an ambient pressure of 0.5–1.0 Pa using 12 SCCM nitrogen and 14 SCCM Ar-diluted SiH_4. As the substrates were unintendedly heated during film deposition, the actual deposition temperature was measured lower than 50 °C, depending on the deposition rate, thus mentioned as room-temperature deposition in this study following convention. Fourier transform infrared spectroscopy (FTIR, NICOLET 6700) was used to study the vibrational modes within 400 to 4000 cm^{-1} in the films deposited at different input powers, as shown in Fig. 10. The assignments for these modes are (1) N—H stretching mode at ~3330 cm^{-1}, (2) Si—H stretching at ~2140 cm^{-1}, (3) N—H and N—H_2 bending at ~1150 cm^{-1}, (4) Si—N stretching between 870 and 820 cm^{-1}. No Si—O related feature was observed at 1050 cm^{-1}. The Si—N stretching mode was not obviously shifted, suggesting that the hydrogen content in the films does not strongly depend on the input power, because the Si—N stretching mode is very sensitive to the bonding environment of hydrogen [31,39]. Using the absorption cross sections for Si—H and N—H sites determined by Langford and Rand [40], the hydrogen density in the films was estimated to be $1.0 \pm 0.2 \times 10^{22}$ cm^{-3}, with more than 90% of this bonded to N. With the decrease in the nitrogen dissociation degree, the hydrogen bonded to Si was slightly increased. By increasing the ambient pressure, the hydrogen content could be further decreased below 5×10^{21} cm^{-3}, suggesting that the hydrogen concentration would be reduced lower than 5%.

Atomic force microscopy (AFM, SPM 5000, Benyuan) was used to study the morphology and roughness of the a-SiN_x:H films. The AFM images revealed that the a-SiN_x:H films exhibit a dense structure with smooth surface, as shown in Fig. 11. The film roughness was determined to be in sub-nanometer scale within the 1 μm × 1 μm AFM images, as shown in Fig. 12(a), indicating that the a-SiN_x:H films are potential in

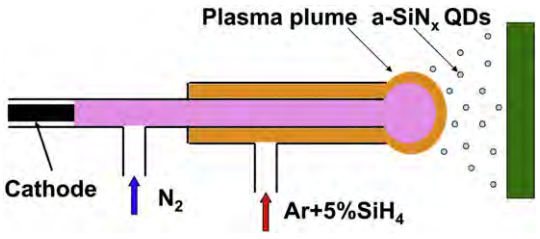

Fig. 9. Schematic diagram for the synthesis of a-SiN_x:H and a-SiN_x:H QD films.

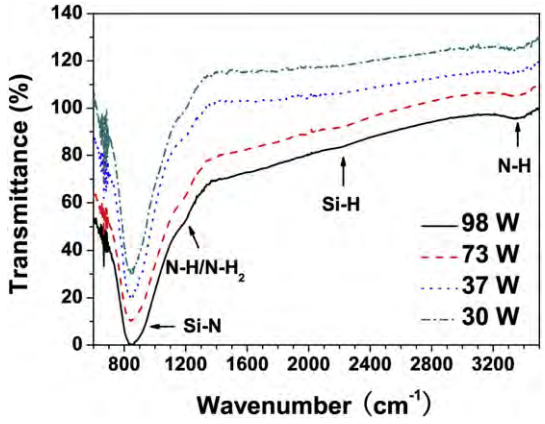

Fig. 10. FTIR spectra in wavenumbers ranging 400 to 4000 cm^{-1} for the films deposited at the given input powers.

the applications of opto-electronic devices. The deposition rate in Fig. 12(a) was determined using the film thickness by fitting the reflectance of the films deposited at the given time, as shown in Fig. 12(b). The results clearly show that the deposition rate is definitely associated with the dissociation degree of nitrogen in the plasma, differing from the conclusions obtained by changing the energy of N_2^+ ions and the duty ratio of the pulsed PECVD in the previous studies of *a*-SiN_x:H deposition [41]. When increasing the dissociation degree from 2.4% to 10.5%, the deposition rate increases from 35 to 104 nm/min, which is sufficiently high for industrial applications. Furthermore, the tubular plasma source has the advantage easily integrating into a large-scale array to fit the shapes of various work-pieces. The high rate of *a*-SiN_x:H deposition at room temperature is attributed to the high dissociation degree of nitrogen. On the other hand, the relatively high temperature of neutrals in the plasma, which is in the range of 350–700 K and higher than that in glow discharge, promotes the formation of *a*-SiN_x:H in the plume.

4. Conclusions

A high activity of nitrogen plasma is created at low pressure using a tubular plasma source driven by low-frequency AC generator. The discharge in the tube is recognized with a low-frequency driving continue discharge comprising periodically pulsed discharge, which is associated with ionization wave. Excited at the input power of 10 to 115 W, the discharge allows loading a power density as high as ~80 W/cm^3 to the plasma, thus producing high activity of nitrogen plasma. The nitrogen dissociation degree in the tube is determined to be dependent on the power density and more than 10% dissociation degree has been achieved. Based on the high activity of nitrogen plasma, a special PECVD system was designed for deposition of *a*-SiN_x:H films. By separately feeding working gases of pure nitrogen and Ar-diluted 5% silane, low H-content *a*-SiN_x:H films were successfully deposited at room temperature, with a sufficient deposition rate higher than 100 nm/min.

Acknowledgement

The EELS analysis and the partial TEM work was done at International Center for Dielectric Research (ICDR), Xi'an Jiaotong University, Xi'an,

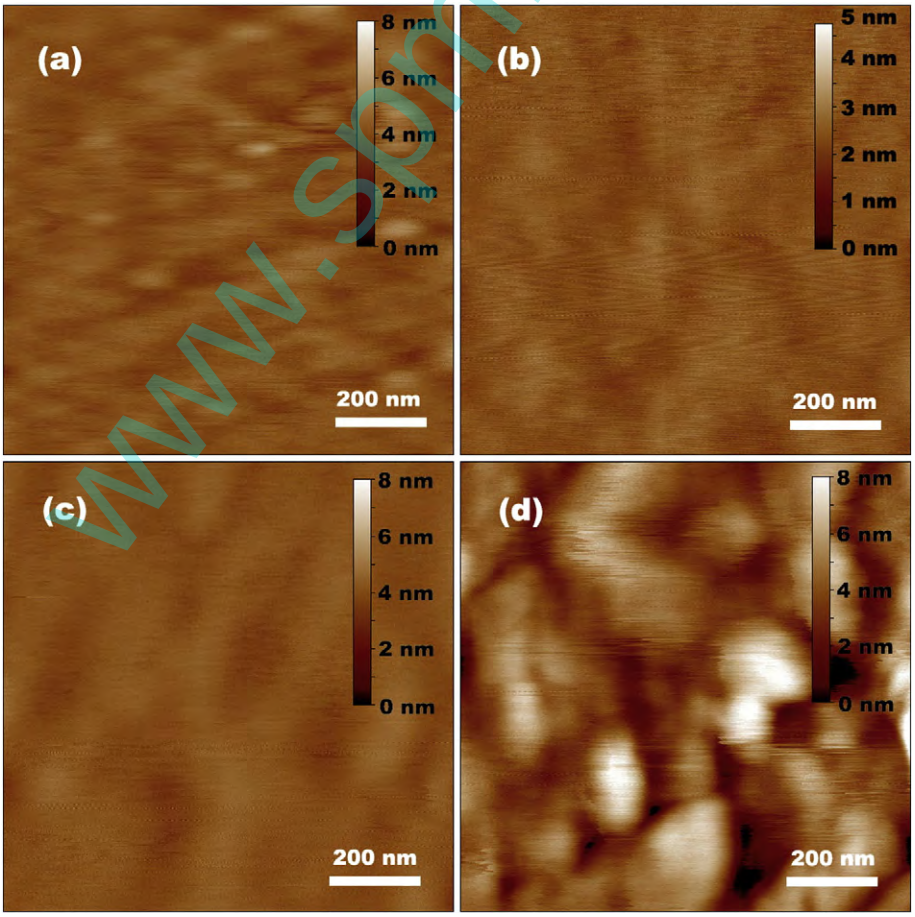

Fig. 11. 1 μm × 1 μm AFM images of the *a*-SiN_x:H films deposited at 98 W (a), 73 W (b), 37 W (c), and 30 W (d).

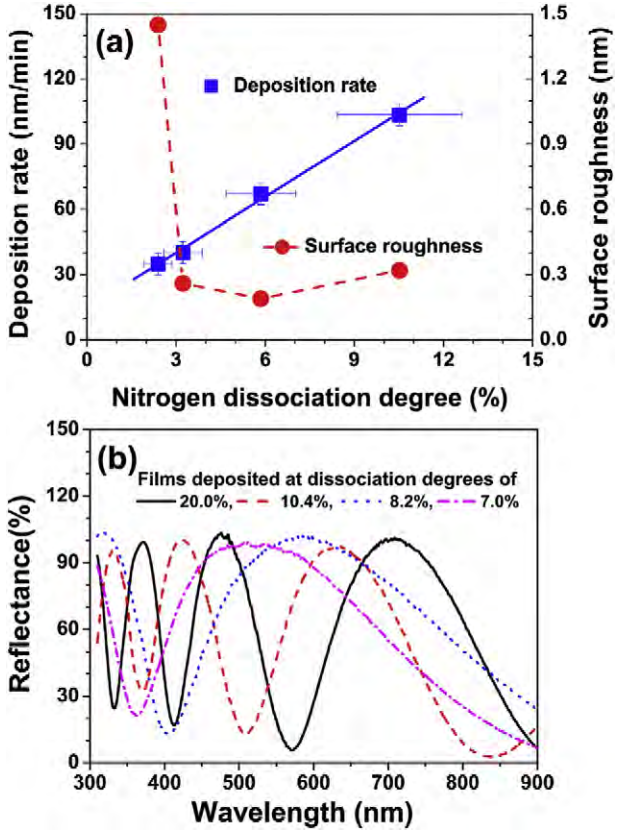

Fig. 12. (a) Deposition rate and surface roughness of the *a*-SiN_x:H film plotted as a function of nitrogen dissociation degree. (b) Reflectance of the *a*-SiN_x:H film deposited at the given dissociation degrees. The deposition time was 4 min for the dissociation degrees of 20.0%, 8.2%, and 7.0%, and 5 min for the dissociation degree of 10.4%. The reflectance was measured with respect to a Si wafer same as the Si substrates.

China. The authors also thank Dr. Lu Lu for her help in EELS analysis and using TEM. One of authors, Q. Y. Zhang, thanks Prof. X. Q. Wen in Dalian University of Technology for his discussion in the plasma discharge.

References

[1] K.H. Becker, K.H. Schoenbach, J.G. Eden, Microplasmas and applications, J. Phys. D. Appl. Phys. 39 (2006) R55–R70.
[2] W. Shi, R.H. Stark, K.H. Schoenbach, Parallel operation of microhollow cathode discharge, IEEE Trans. Plasma Sci. 27 (1999) 16–17.
[3] H. Feng, P. Sun, Y. Chai, G. Tong, J. Zhang, W. Zhu, J. Fang, The interaction of a direct-current cold atmospheric-pressure air plasma with bacteria, IEEE Trans. Plasma Sci. 37 (2009) 121–127.
[4] J.L. Walsh, M.G. Kong, Room-temperature atmospheric argon plasma jet sustained with submicrosecond high-voltage pulses, Appl. Phys. Lett. 91 (2007) 221502.
[5] X.P. Lu, M. Laroussi, Dynamics of an atmospheric pressure plasma plume generated by submicrosecond voltage pulses, J. Appl. Phys. 100 (2006) 063302.
[6] M. Teschke, J. Kedzierski, E.G. Finantu-Dinu, D. Korzec, J. Engemann, High-speed photographs of a dielectric barrier atmospheric pressure plasma jet, IEEE Trans. Plasma Sci. 33 (2005) 310–311.
[7] S.E. Babayan, J.Y. Jeong, A. Schütze, V.J. Tu, M. Moravej, G.S. Selwyn, R.F. Hicks, Plasma Sources Sci. Technol. 10 (2001) 573.
[8] Y. Sakiyama, D.B. Graves, Corona-glow transition in the atmospheric pressure RF-excited plasma needle, J. Phys. D. Appl. Phys. 39 (2006) 3644–3652.
[9] J.J. Shi, M.G. Kong, Mode transition in radio-frequency atmospheric argon discharges with and without dielectric barriers, Appl. Phys. Lett. 90 (2007) 101502.
[10] P. Zhao, W. Zheng, Y.D. Meng, M. Nagatsu, Characteristics of high-purity Cu thin films deposited on polyimide by radio-frequency Ar/H_2 atmospheric-pressure plasma jet, J. Appl. Phys. 113 (2013) 123301.
[11] T. Kikuchi, Y. Hasegawa, H. Shirai, Rf microplasma jet at atmospheric pressure: characterization and application to thin film processing, J. Phys. D. Appl. Phys. 37 (2004) 1537–1543.
[12] J. Kim, K. Terashima, 2.45 GHz microwave-excited atmospheric pressure air microplasmas based on microstrip technology, Appl. Phys. Lett. 86 (2005) 191504.
[13] J. Choi, F. Iza, H.J. Do, J.K. Lee, M.H. Cho, Microwave-excited atmospheric-pressure microplasmas based on a coaxial transmission line resonator, Plasma Sources Sci. Technol. 18 (2009) 025029.
[14] S.Z. Li, M.C. Xu, X. Zhang, J.L. Zhang, A pulse-modulated nonequilibrium atmospheric-pressure microwave argon plasma discharge preionized by a kilohertz excited plasma jet, Appl. Phys. Lett. 100 (2012) 174101.
[15] T. Czerwiec, F. Greer, D.B. Graves, Nitrogen dissociation in a low pressure cylindrical ICP discharge studied by actinometry and mass spectrometry, J. Phys. D. Appl. Phys. 38 (2005) 4278–4289.
[16] T. Czerwiec, D.B. Graves, Mode transitions in low pressure rare gas cylindrical ICP discharge studied by optical emission spectroscopy, J. Phys. D. Appl. Phys. 37 (2004) 2827–2840.
[17] J. Henriques, E. Tatarova, F.M. Dias, C.M. Ferreira, Wave driven N_2–Ar discharge. II. Experiment and comparison with theory, J. Appl. Phys. 91 (2002) 5632–5639.
[18] W.M.M. Kessels, J. Hong, F.J.H. van Assche, J.D. Moschner, T. Lauinger, W.J. Soppe, A.W. Weeber, D.C. Schram, M.C.M. van de Sanden, High-rate deposition of a-SiN_x:H for photovoltaic applications by the expanding thermal plasma, J. Vac. Sci. Technol. A 20 (2002) 1704–1715.
[19] J. Hong, W.M.M. Kessels, F.J.H. van Assche, H.C. Rieffe, W.J. Soppe, A.W. Weeber, M.C.M. van de Sanden, Bulk passivation of multicrystalline silicon solar cells induced by high-rate-deposited (>1 nm/s) silicon nitride films, Prog. Photovolt. Res. Appl. 11 (2003) 125–130.
[20] W.M.M. Kessels, F.J.H. van Assche, J. Hong, D.C. Schram, M.C.M. van de Sanden, Plasma diagnostic study of silicon nitride film growth in a remote Ar–H_2–N_2–SiH_4 plasma: role of N and SiH_n radicals, J. Vac. Sci. Technol. A 22 (2004) 96–106.
[21] H. Pedersen, P. Larsson, A. Aijaz, J. Jensen, D. Lundin, A novel high-power pulse PECVD method, Surf. Coat. Technol. 206 (2012) 4562–4566.
[22] W.C. Zhu, Q. Li, X.M. Zhu, Y.K. Pu, Characteristics of atmospheric pressure plasma jets emerging into ambient air and helium, J. Phys. D. Appl. Phys. 42 (2009) 202002.
[23] C.Y. Miao, D.Q. Shi, C.Y. Ma, C.S. Ren, W.Q. Lu, Q.Y. Zhang, C. Zhang, Z. Yi, Mode transition and related discharge phenomena of a tube plasma source operating in low-pressure pure nitrogen atmospher, IEEE Trans. Plasma Sci. 43 (2015) 544–551.
[24] P. Vidaud, S.M.A. Durrani, D.R. Hall, Alpha and gamma RF capacitance discharges in N_2 at intermediate pressures, J. Phys. D. Appl. Phys. 21 (1988) 57–66.
[25] A. Lofthus, P.H. Krupenie, The spectrum of molecular nitrogen, J. Phys. Chem. Ref. Data 6 (1977) 113–307 (or the calculated data with the data provided here).
[26] http://physics.nist.gov/asd (or the calculated data with the data provided here).
[27] R.M. Frost, P. Awakowicz, H.P. Summers, N.R. Badnell, Calculated cross sections and measured rate coefficients for electron-impact excitation of neutral and singly ionized nitrogen, J. Appl. Phys. 84 (1998) 2989–3003.
[28] Y. Itikawa, Cross sections for electron collisions with nitrogen molecules, J. Phys. Chem. Ref. Data 35 (2006) 31–53.
[29] V. Guerra, P.A. Sá, J. Loureiro, Kinetic modeling of low-pressure nitrogen discharges and post-discharges, Eur. Phys. J. Appl. Phys. 28 (2004) 125–152.
[30] Q.Y. Zhang, D.Q. Shi, W. Xu, C.Y. Miao, C.Y. Ma, C.S. Ren, C. Zhang, Z. Yi, Determination of vibrational and rotational temperatures in highly constricted nitrogen plasmas by fitting the second positive system of N_2 molecules, AIP Adv. 5 (2015) 057158.
[31] G.N. Parsons, J.H. Souk, J. Batey, Low hydrogen content stoichiometric silicon nitride films deposited by plasma enhanced chemical vapor deposition, J. Appl. Phys. 70 (1991) 1553–1560.
[32] M.A. Pereira, J.A. Diniz, I. Doi, J.W. Swart, Silicon nitride deposited by ECR-CVD at room temperature for LOCOS isolation technology, Appl. Surf. Sci. 212 (2003) 388–392.
[33] F.Z. Liu, S. Ward, L. Gedvilas, B. Keyes, B. To, Q. Wang, E. Sanchez, S.L. Wang, Amorphous silicon nitride deposited by hot-wire chemical vapor deposition, J. Appl. Phys. 96 (2004) 2973–2979.
[35] S. Kim, B. Kim, Radio frequency bias power effects on silicon nitride film deposited in SiH_4–NH_3 using a plasma-enhanced chemical vapor deposition, Met. Mater. Int. 15 (2009) 881–885.
[35] L.D.S. Zambom, R.D. Mansano, A.P. Mousinho, Low-temperature deposition of silicon oxide and silicon nitride by reactive magnetron sputtering, Microelectron. J. 40 (2009) 66–69.
[36] B. Kim, S. Kim, Radio frequency source power effect on silicon nitride films deposited by a room-temperature pulsed-PECVD, Thin Solid Films 517 (2009) 4090–4093.
[37] A. Kshirsagar, P. Nyaupane, D. Bodas, S.P. Duttagupta, S.A. Gangal, Deposition and characterization of low temperature silicon nitride films deposited by inductively coupled plasma CVD, Appl. Surf. Sci. 257 (2011) 5052–5058.
[38] A. El Amrani, A. Bekhtari, B. Mahmoudi, A. Lefgoum, H. Menari, Experimental study of the effect of process parameters on plasma-enhanced chemical vapour deposition of silicon nitride film, Vacuum 86 (2011) 386–390.
[39] E.A. Taft, Characterization of silicon nitride films, J. Electrochem. Soc. 118 (1971) 1341–1346.
[40] W.A. Lanford, M.J. Rand, The hydrogen content of plasma deposited silicon nitride, J. Appl. Phys. 49 (1978) 2473–2477.
[41] D.Y. Kim, B.W. Kim, N.G. Yoon, Duty ratio impact on SiN films deposited in SiH_4–NH_3 plasma at room temperature, Microelectron. Eng. 89 (2012) 116–119.